# Adenosine Triphosphate-Triggered Release of Macromolecular and Nanoparticle Loads from Aptamer/DNA-Cross-Linked Microcapsules

**Wei-Ching Liao,[†] Chun-Hua Lu,[†] Raimo Hartmann,[‡] Fuan Wang,[†] Yang Sung Sohn,[§] Wolfgang J. Parak,[*,‡] and Itamar Willner[*,†]**

[†]Institute of Chemistry, Center for Nanoscience and Nanotechnology, The Hebrew University of Jerusalem, Jerusalem 91904, Israel, [‡]Fachbereich Physik, Philipps-Universität Marburg, Renthof 7, 35037 Marburg, Germany, and [§]Institute of Life Science, The Hebrew University of Jerusalem, Jerusalem 91904, Israel

**ABSTRACT** The synthesis of stimuli-responsive DNA microcapsules acting as carriers for different payloads, and being dissociated through the formation of aptamer—ligand complexes is described. Specifically, stimuli-responsive anti-adenosine triphosphate (ATP) aptamer-cross-linked DNA-stabilized microcapsules loaded with tetramethylrhodamine-modified dextran (TMR-D), CdSe/ZnS quantum dots (QDs), or microperoxidase-11 (MP-11) are presented. In the presence of ATP as trigger, the microcapsules are dissociated through the formation of aptamer—ATP complexes, resulting in the release of the respective loads. Selective unlocking of the capsules is demonstrated, and CTP, GTP, or TTP do not unlock the pores. The ATP-triggered release of MP-11 from the microcapsules enables the MP-11-catalyzed oxidation of Amplex UltraRed by $H_2O_2$ to the fluorescent product resorufin.

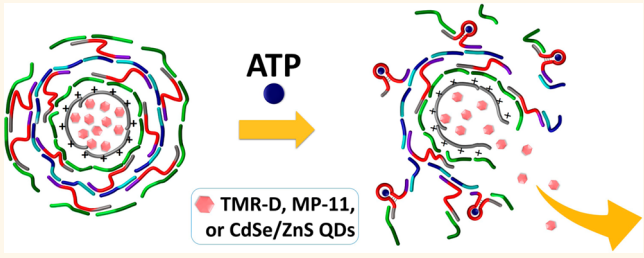


**KEYWORDS:** controlled release · biocatalyst · quantum dot (QD) · microperaoxidase-11 · fluorescence

The fabrication of layer-by-layer microcapsules with encapsulated macromolecular loads to yield microcarriers for controlled release attracts substantial research efforts.[1−5] One method to prepare the substrate-loaded microcapsules involves the coprecipitation of macromolecular loads with inorganic $CaCO_3$ microparticles acting as core-templates. The coating of the micrometer-sized core template particles with a shell and the subsequent dissolution of the core templates yield the substrate-loaded microcapsules. Different methods to assemble the coating shell on the template core were reported, and these include electrostatic layer-by-layer deposition of polyelectrolytes,[6−10] the use of biorecognition complexes as interlayer linking units,[11] and the use of covalent bonds to bridge the layers,[12,13] *e.g.*, disulfide bonds as interlayer bridges.[14] Several methods for the controlled release of the loads were reported, and these include the thermal degradation of the microcapsules by light-induced local heating of entrapped plasmonic nanoparticles,[15−19] by local heating stimulated by alternating magnetic fields acting on entrapped magnetic nanoparticles,[20] by mechanical agitation using ultrasound[21−23] or microwaves,[24] and by the use of magnetic fields to rotate the nanoparticles.[25] Also, chemical stimuli, such as pH,[26] salts,[27] gases,[28] carbohydrates,[29] or the reduction of disulfide bridging units,[30] and the application of enzymes as catalysts for the decomposition of biodegradable shells,[31−33] were used to separate the shells, and stimulate the release of the cargoes from the microcapsules. Different applications of substrate-loaded microcapsules were suggested. These include the use of functionalized microcapsules as sensors,[34,35] and as microreactors for biocatalytic reactions,[36−38] and specifically, the use of substrate-loaded microcapsules for biomedical applications, such as drug delivery[39−41] and imaging[42] systems.

The base pairing of nucleotides provides a means to construct DNA-based microcapsules.

* Address correspondence to willnea@vms.huji.ac.il, wolfgang.parak@physik.uni-marburg.de.

Received for review May 28, 2015 and accepted August 12, 2015.

**Published online August 12, 2015**
10.1021/acsnano.5b03223

Substrate-loaded microcapsules consisting of DNA layers interlinked by hybridization bridges were reported.[43−46] The use of DNA as a stabilizing shell for microcapsules is particularly interesting, since recognition or catalytic properties of DNA can encode stimuli-responsive functions into the DNA shell that lead to the degradation of the capsules.[47] Indeed, by programming the base sequences of the interlinked hybridized DNA layers, the site-specific degradation of DNA capsules by restriction enzymes and the release of enzyme loads were demonstrated.[48] Aptamers are sequence-specific nucleic acids that recognize low-molecular-weight substrates, macromolecules and even cells.[49−52] It was demonstrated that by the appropriate design of the nucleic acid sequences, duplex DNA domains can be separated by the formation of energetically stabilized aptamer−ligand complexes.[53−57] Previous studies have demonstrated the assembly of aptamer-funcitonalized polyelectrolyte-based microcapsules for controlled release[58,59] and sensor[60] applications. Specifically, the formation of aptamer−ligand complexes provides the stimuli-responsive mechanism for the rupture of the microcapsules. In the present study, we demonstrate the novel preparation of stimuli-responsive DNA microcapsules consisting of oligonucleotide layers cross-linked by an anti-ATP aptamer sequence. In the presence of adenosine triphosphate (ATP), the resulting ATP aptamer complex fragments the DNA shell, resulting in the release of encapsulated macromolecular, biomolecular or nanoparticle cargoes. The ATP-responsive capsules are of specific interest since ATP is overexpressed in certain diseases, *e.g.*, in cancer cells,[61,62] and thus, the ATP-responsive capsules might facilitate the release of drugs in targeted cells. Furthermore, we demonstrate the selective ATP-driven release of semiconductor quantum dots or the microperoxidase-11 biocatalyst, thus providing versatile means to selectively release functional payloads from the ATP-responsive microcapsules. The key point of the study is reflected by the introduction of a new, nonenzymatic, mechanism for the degradation of DNA microcapsules using aptamer−ligand complexes. This mechanism would allow sense-and-treat therapeutic treatments.

## RESULTS AND DISCUSSION

Figure 1 outlines the stepwise preparation of the ATP aptamer-cross-linked DNA microcapsules. Template $CaCO_3$ particles (~3.2 $\mu$m diameter) were loaded with tetramethylrhodamine-modified dextran, TMR-D, using a coprecipitation method following a reported procedure.[63] The particles were coated with a primary layer of the positively charged polyelectrolyte, poly(allylamine hydrochloride) PAH (58 kDa). The nucleic acid, hybrid **1**/**2** was then used as a first DNA, negatively charged, coating layer on the PAH-modified particles. Note that the hybrid **1**/**2** includes two units of **1** that bind to **2**. The strand **1** includes two subdomains A and B, and the hybridization of the two units of **1** with **2** proceeds *via* specific hybridization directionality of the subdomains to **2**. Also, note that the sequence **2** includes the ATP aptamer sequence marked in red color. Subsequently, a hybrid composed of **3** and **2** was hybridized with the first DNA coating layer to yield a second layer. Similarly, the **3**/**2** hybrid includes two units of **3** that are hybridized with **2** through subdomains C and D. The single-stranded 3′ subdomains of **2** on the first layer are complementary to the single-stranded free tether C and D of **3**, resulting in the hybridization and cross-linking of the second DNA layer on the particles. By the sequential treatment of the microparticles with the hybrids **1**/**2** and **3**/**2**, a controlled number of DNA layers were constructed on the $CaCO_3$ template particles. (For the detailed sequence composition of **1**, **2**, and **3**, and their specific interhybridization feature leading to the formation of the layers, see Figure 1, bottom.) The resulting particles were then treated with EDTA to dissolve the core $CaCO_3$ template by forming a water-soluble complex with $Ca^{2+}$ ions, resulting in the TMR-D-entrapped DNA capsules. It should be noted that the primary PAH layer is essential to form the capsules. Presumably, the positive charge associated with PAH enables the efficient coating of a template by the **1**/**2** units and the subsequent build-up of the layers. Also, it should be noted that the formation of the $Ca^{2+}$−EDTA complex prevents the interaction of free $Ca^{2+}$ ions with the DNA shell and the aggregation of the microcapsules.

Figure 2 depicts the characterization of the capsules. In Figure 2A, the scanning electron microscopy (SEM) images of the, as prepared, $CaCO_3$ core template particles, panel I, the DNA-coated $CaCO_3$ template, panel II, and the capsules generated upon dissolution of the $CaCO_3$ core, panel III, are presented. While the uncoated $CaCO_3$ particles (~3.2 $\mu$m diameter) exhibit a smooth, porous surface, the DNA-coated template particles show a rough "hairy" surface, indicating the assembly of the DNA layers. After the dissolution of the $CaCO_3$ core, collapsed spheres were observed, indicating the hollow nature of the DNA capsules and complete removal of the core. Note that this collapse is due to the vacuum conditions, yet in water the capsules remain in an intact spherical shape (for other collapsed microcapsules, see Figure S1). Figure 2B shows the fluorescence and bright-field microscopy images of the DNA capsules upon their preparation. The DNA-coated core $CaCO_3$ TMR-D-impregnated particles show high-fluorescence intensity images, and from overlapping bright-field images, sizes of *ca.* 3.2 $\mu$m can be deducted (panel I). Treatment of the particles with EDTA yields fluorescent capsules that can be imaged also by bright-field microscopy (panel II). The removal of core causes the shrinkage of capsules, and the average diameter was reduced to about 2.5 $\mu$m.

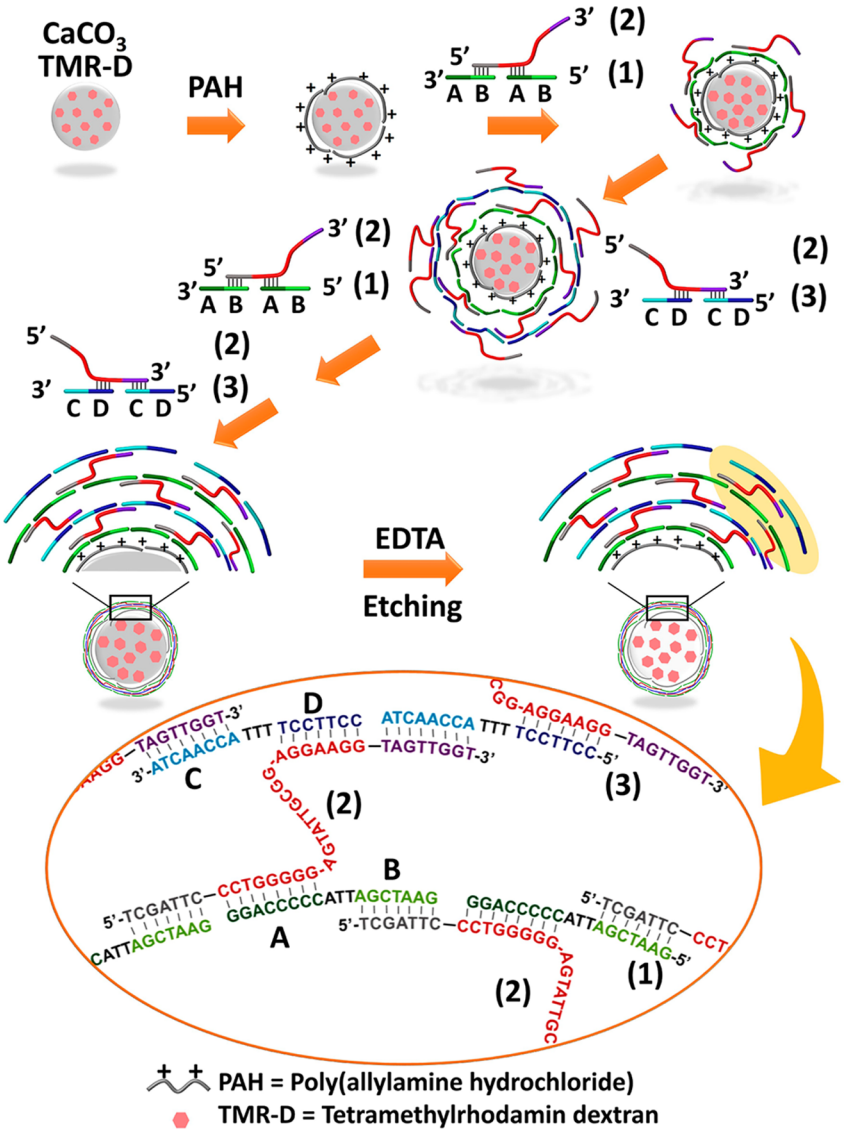


**Figure 1. Schematic illustration of the preparation process of DNA microcapsules by using $CaCO_3$ as template and the subsequent layer-by-layer DNA assembly. ATP-binding aptamer sequences labeled in red color are embedded into DNA films as stimuli-sensitive switches.**

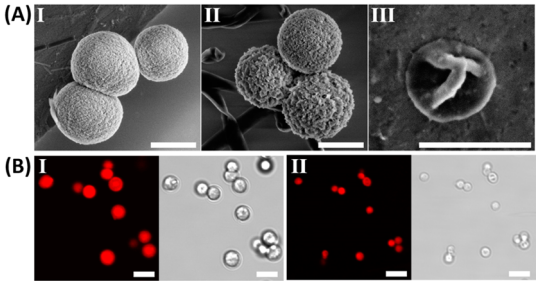


**Figure 2. (A) SEM images of uncoated $CaCO_3$ particles (I), DNA-coated $CaCO_3$ particles before (II) and after (III) EDTA treatment. Scale bar is 2 $\mu$m. (B) Confocal fluorescence and bright-field microscopy images of DNA-coated $CaCO_3$ particles before (I) and after (II) EDTA treatment. Scale bar is 5 $\mu$m.**

From the number of DNA layers and the composition of the shell, we estimate that the thickness of the shells is *ca.* 35−40 nm. The fluorescence of the resulting capsules is, however, lower, indicating that in the process of the core dissolution some of the TMR-D fluorescent labels leaked out of the capsules. This is due to the semiporosity of the capsules walls, which imposes a molecular-weight-dependent filter for diffusion.[63] The resulting capsules were stable for at least 3 days, and their fluorescence and features were unchanged even upon the repeated washing of the capsules with a buffer solution.

The schematic unlocking of the capsules and the triggered release of the entrapped TMR-D are schematically presented in Figure 3A. The addition of ATP to the capsules is anticipated to stimulate the formation of the energetically stabilized ATP-aptamer complexes. As a result, the bridging units of the DNA coating should be disrupted, resulting in the dissolution of parts of the coating and the release of TMR-D. Figure 3B depicts the confocal fluorescence and bright-field

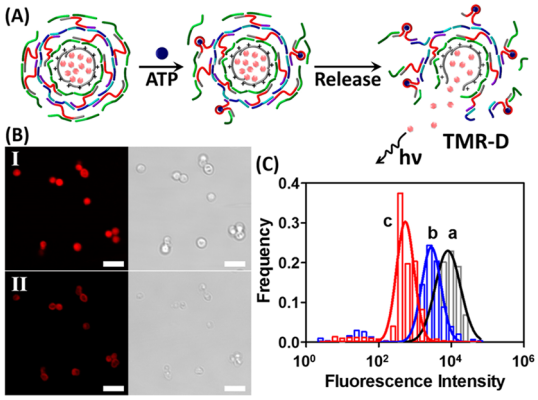


**Figure 3. (A) Schematic representation of ATP-induced capsules unlocking and entrapped TMR-D releasing. (B) Confocal fluorescence and bright-field microscopy images of DNA capsules before (I) and after (II) ATP treatment. Scale bar is 5 $\mu$m. (C) Fluorescence intensity distributions corresponding to (a) the DNA-coated $CaCO_3$ particles; (b) the EDTA-treated particles; (c) the ATP-treated capsules. Fluorescence intensities for all systems were measured by flow cytometry after a fixed time-interval of 3 h. All samples were incubated in 10 mM HEPES buffer solution including 500 mM NaCl, pH = 7.0 for a fixed time-interval of 3 h prior to the measurement.**

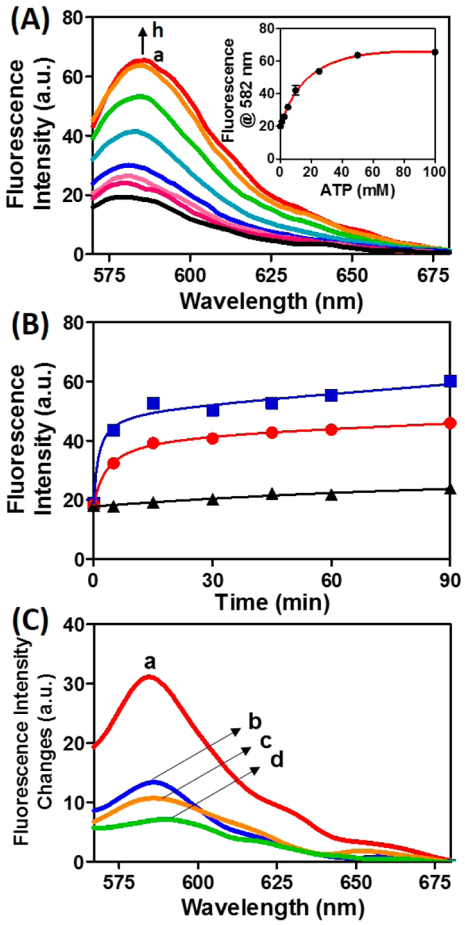


**Figure 4. (A) Fluorescence spectra of the released dye upon the addition of various concentration of ATP into the DNA capsules solution: (a) 0, (b) 1, (c) 2.5, (d) 5, (e) 10, (f) 25, (g) 50, and (h) 100 mM. The release of the fluorescent dye into the solution is monitored after a fixed time interval of 30 min. (Inset) Calibration curve corresponding to the fluorescence changes upon the release of TMR-dextran from the capsules. (B) Fluorescence releasing profile of the DNA capsules upon treatment with 25 mM (■), 10 mM (●), and 0 mM (▲) ATP. Lines are to guide the eye only. (C) Changes in fluorescence spectra of released dye in capsules upon the treatment with 25 mM of ATP (a), TTP (b), CTP (c), and GTP (d) subtracted from the background fluorescence of untreated capsules.**

microscopy images of the microcapsules before addition of ATP, panel I, and after addition of ATP, 100 mM, and allowing the capsules to interact with ATP for a time interval of 15 min, panel II. Clearly, a decrease in fluorescence intensity of the ATP-treated microcapsules was observed; meanwhile, the capsules under bright-field were almost invisible. These results suggest that ATP, indeed, dissolved parts of the DNA domains of the shells, and the resulting pores allowed the release of the TMR-D. Further support for the effects of core dissolution and addition of ATP on the release of TMR-D from the capsules was obtained from flow cytometry experiments, Figure 3C. The DNA-coated TMR-D-impregnated $CaCO_3$ particles show high fluorescence. The EDTA-treated particles reveal a substantially lower fluorescence intensity, consistent with the partial leakage of TMR-D during the dissolution of the core. The ATP-treated microcapsules show a substantially lower fluorescence intensities, confirming the ATP-driven release of TMR-D from the DNA-functionalized microcapsules.

The effectiveness of the release of TMR-D from the capsules is controlled by the time-intervals and the concentrations of ATP to which the capsules are subjected. Figure 4A depicts the fluorescence spectra of the released TMR-D upon exposing the microcapsules to variable concentrations of ATP for a fixed time-interval of 30 min. In these experiments, samples containing an equal number of TMR-D loaded capsules were treated with different concentrations of ATP for a fixed time interval of 30 min. The resulting samples were centrifuged to precipitate the residual capsules, and the fluorescence of the released TMR-D in the supernatant solution was assayed. As the concentration of ATP rises, a higher content of TMR-D is released, and the released TMR-D reaches a saturation value at *ca.* 50 mM of ATP Figure 4(A), inset. From the fluorescence intensity of the released TMR-D, and knowing the number of microcapsules in the sample, we estimate that an average number of *ca.* $2.3 \times 10^{-16}$ mol of TMR-D was released from each particle. Figure 4B depicts the rate of release of TMR-D from the capsules exposed to different concentrations of ATP. In these experiments, samples containing an identical content of capsules were subjected to variable concentrations of ATP, and the content of released TMR-D, at different time-intervals of interaction with ATP, was monitored by precipitation of the capsules and monitoring the fluorescence of released TMR-D. As the concentration of ATP increases, the release

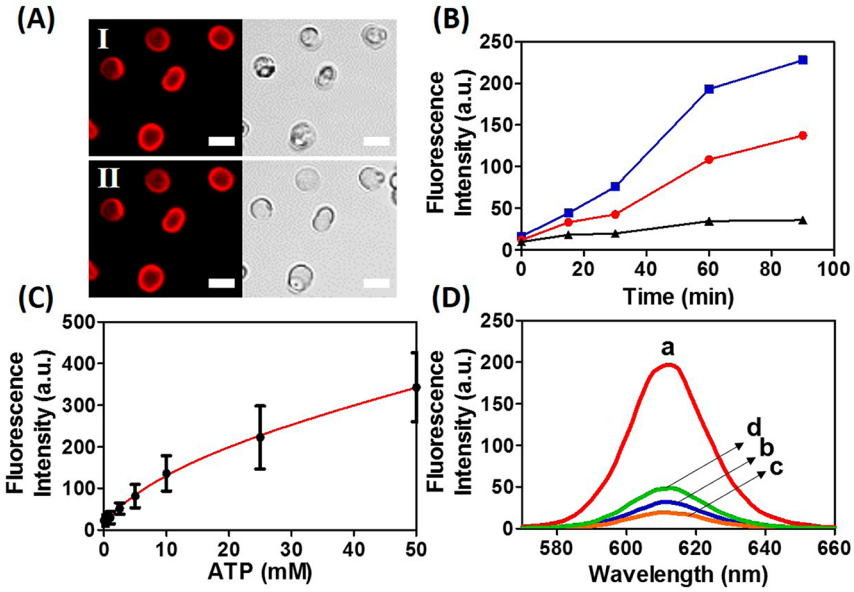


**Figure 5. (A) Confocal fluorescence and bright-field microscopy images of the CdSe/ZnS QDs-loaded particles before (I) and after (II) EDTA treatment. Scale bar is 5 $\mu$m. (B) Fluorescence releasing profile of DNA capsules treated with 25 mM (■), 10 mM (●), and 0 mM (▲) ATP. (C) Calibration curve corresponding to the fluorescence changes upon release of CdSe/ZnS QDs from the capsules. (D) Fluorescence spectra of the released CdSe/ZnS QDs from the capsules upon the treatment with 25 mM of ATP (a), TTP (b), CTP (c), and GTP (d).**

of TMR-D is faster, consistent with the enhanced degree of separation of the DNA shell through the formation of the ATP–aptamer complexes. Finally, we addressed the selectivity toward the ATP-triggered release of TMR-D from the capsules. Figure 4C depicts the changes in fluorescence spectra of the TMR-D released from ATP-treated capsules, curve a, and capsules subjected to other nucleoside triphosphates, guanosine triphosphate, GTP, cytidine triphosphate, CTP, and thymidine triphosphate, TTP, compared to the background intensity of untreated capsules. Evidently, only ATP stimulates the effective release of TMR-D, and the other triphosphates yield only background fluorescence levels, similar to the untreated microcapsules. The residual fluorescence observed with the untreated microcapsules or the GTP-, CTP-, TTP-treated microcapsules is attributed to the physical partial disruption of a small fraction of the capsules upon their centrifugation and separation. Further support for the selective dissociation of the aptamer-cross-linked microcapsules through the formation of the aptamer–ATP complex was obtained by applying a nonaptameric sequence **2a** for the construction of the microcapsules, Figure S2. One may realize that addition of ATP does not unlock the microcapsules cross-linked by nonaptameric bridges. Thus, the selectivity of the ATP-triggered release of TMR-D from the capsules is attributed to the selectivity of the aptamer bridges toward ATP. That is, only the formation of the ATP–aptamer complex fragments the DNA shell of the microcapsules.

The ATP-responsive microcapsules were further loaded with mercaptopropionic acid-functionalized CdSe/ZnS quantum dots (QDs). Figure 5A depicts the confocal fluorescence and bright-field microscopy images of the CdSe/ZnS QDs-loaded capsules. In these experiments, the QDs/$CaCO_3$ loaded capsules were fixed on the glass support and imaged by fluorescence microscopy and bright-field microscopy, before and after treatment of the capsules with EDTA (image I and II, respectively). The bright-field microscopy images reveal that the $CaCO_3$ cores are present in the capsules prior to the treatment with EDTA (dark dots), whereas after treatment with EDTA, the cores are dissolved evident by transparent core regions. The fluorescence features of the microcapsules are, however, similar before and after treatment with EDTA, implying that the QDs are localized in the microcapsules. Figure 5B shows the time-dependent fluorescence changes of the released QDs upon the treatment of the capsules with variable concentrations of ATP. Figure 5C shows the ATP concentration-dependent release of the CdSe/ZnS QDs at a fixed time interval of 60 min. As the concentration of ATP increases, the fluorescence of the released QDs is intensified, consistent with the higher degree of unlocking of the microcapsules. The release of the QDs from the microcapsules is selective. Figure 5D depicts the fluorescence spectra of the QDs released upon subjecting the microcapsules to ATP, TTP, CTP and GTP for a fixed time interval of 60 min. Evidently, only the ATP triggers the effective release of the QDs, consistent with the selective dissociation of the microcapsule shells through the formation of the ATP–aptamer complex that removes the aptamer bridging units. From the fluorescence intensity of the QDs observed upon treatment of the capsules with ATP, 25 mM, for a time-interval of 60 min, we conclude that *ca.* 358 fmol of CdSe/ZnS QDs were released.

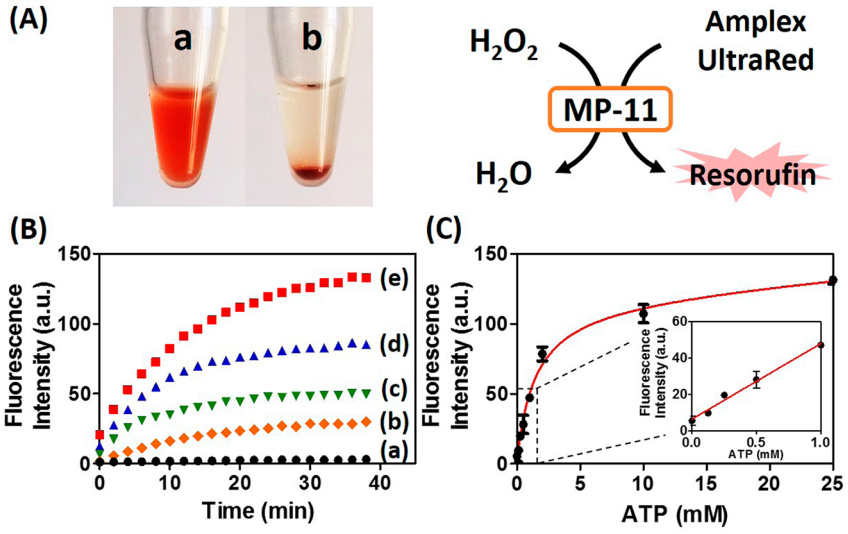


**Figure 6. (A) Photograph of the suspension of DNA-coated MP-11-encapsulated $CaCO_3$ particles (a) and of the precipitate after centrifugation (b). (B) Probing the ATP-simulated release of MP-11 from the capsules by following the fluorescence changes induced by the MP-11-catalyzed oxidation of Amplex UltraRed to resorufin in the presence of $H_2O_2$. In these experiments, the capsules were treated with a constant concentration of ATP, 25 mM, and the MP-11 load was allowed to be released from the capsules for different time-intervals corresponding to (a) 0, (b) 5, (c) 15, (d) 30, (e) 60 min. The capsules were precipitated after the stated time-intervals of release and the resulting MP-11-catalyzed oxidation of Amplex UltraRed by $H_2O_2$ using fluorescence spectroscopy was applied to follow the activity (content) of MP-11. (C) Calibration curve corresponding to the fluorescence changes of the generated resorufin upon release of MP-11 from the capsules at a fixed time interval of 60 min.**

It should be noted that for the different systems the number of layers comprising the microcapsules had to be optimized. We find that the PAH/nucleic acid shell of the microcapusles, presumably, interacts with the payloads incorporated in the microcapsules. These interactions control the stabilities and permeabilities of the microcapsules toward the release of the loads in the absence of ATP. That is, for each of the systems, we had to tune the number of aptamer-cross-linked DNA layer to the extent that optimal efficiencies of the ATP-driven release of the loads as compared to the background nontriggered release of the loads are obtained. This is exemplified in Figure S3, demonstrating that for the TMR-D load, an optimal release efficiency is obtained for microcapsules consisting of six aptamer-bridged layers. In contrast, for the CdSe/ZnS QDs as load, an optimal release efficiency is observed with microcapsules composed of three aptamer-bridged layers, Figure S4. Further support for the stepwise assembly of the **2**-cross-linked DNA layers on the PAH base layer and the selective ATP-driven dissociation of the layer structure was obtained by complementary quartz-crystal-microbalance (QCM) experiments, Figure S5. In these experiments, a Au/quartz piezoelectric crystal (9 MHz) was functionalized with a mercaptopropionic acid monolayer, and PAH was deposited on the monolayer-functionalized crystal. By a stepwise process, the **1**/**2** and **3**/**2** DNA duplexes were deposited on the base PAH layer. Figure S5A depicts the changes in the crystal frequency upon the build-up of the layers. While the assembly of mercaptopropionic acid as the surface resulted in a frequency change of $\Delta f = -6$ Hz, the association of PAH yielded a frequency change of $\Delta f = -110$ Hz. The first three layers of the DNA led to an average frequency change of *ca.* $-79$ Hz that translates to a surface coverage of *ca.* $1.8 \times 10^{-11}$ mol·cm$^{-2}$ of **1**/**2** or **3**/**2** per layer. The selective ATP-driven dissociation of the layered DNA structure is presented in Figure S5B. Treatment of the layered **1**/**2**, **3**/**2** DNA structure (six layers) resulted in an increase in the crystal frequency of *ca.* 200 Hz, consistent with the rupture of most of DNA layers from the surface. Also, Figure S5B confirms the selectivity of the ATP-triggered separation of the layered structure, and CTP, TTP or GTP result in a minute separation ($<-50$ Hz) of DNA from the interface.

Similarly, microperoxidase-11, MP-11, a heme-containing peptide that mimics the catalytic functions of cytochrome C, was incorporated as load into the ATP-responsive microcapsules. Figure 6A shows the photograph of the MP-11-loaded $CaCO_3$ particles coated with ATP-stimuli sensitive DNA coating. The red color of the suspension (left) corresponds to the MP-11-loaded particles. After centrifugation, the particles were precipitated (right) resulting in an almost colorless solution, implying that the MP-11 was fully integrated with the DNA coated $CaCO_3$ particles. After treatment of the particles with EDTA and the dissolution of the $CaCO_3$ core, the intact red-colored microcapsules were generated. The ATP-triggered release of MP-11 from the microcapsules was followed by probing the catalytic activity of the released MP-11 by analyzing the $H_2O_2$-mediated MP-11 catalyzed oxidation of Amplex UltraRed to the fluorescent product resorufin.[64] Figure 6B depicts the time-dependent fluorescence changes observed upon the

biocatalyzed oxidation of Amplex UltraRed by $H_2O_2$ by the MP-11 released from the microcapsules at different time intervals in the presence of ATP, 25 mM. It should be noted that the MP-11-loaded microcapsules did not show any background leakage of MP-11 in the absence of ATP. Even after a time-interval of 3 h, no MP-11 activity in the supernatant solution toward the oxidation of Amplex UltraRed could be detected. Using an appropriate calibration curve, we evaluated the concentration of the released MP-11 from the capsules, in the presence of added ATP, 25 mM, and after a time-interval of 60 min, to be 11 $\mu g \cdot mL^{-1}$. Similarly, Figure 6C shows the time-dependent fluorescence changes of resorufin ($\lambda = 582$ nm), generated by the MP-11-catalyzed oxidation of Amplex UltraRed by $H_2O_2$, where the MP-11 is released from the capsules in the presence of variable concentrations of ATP for a fixed time interval of 60 min. As the concentration of ATP is higher, the content of released MP-11 increases, resulting in the faster oxidation of Amplex UltraRed by $H_2O_2$.

## CONCLUSIONS

In conclusion, the present study has demonstrated an aptamer-based paradigm to assemble functional, stimuli-responsive, DNA-based capsules for the triggered release of loads. Since the arsenal of sequence-specific aptamers is very broad, the design of other ligand-triggered microcapsules can be envisaged. Furthermore, by mixing microcapsules that include different loads, and the subsequent ligand-induced unlocking and release of target loads, programmed synthesis, the activation of pro-drugs, or the activation of dictated catalytic cascades should be possible. The ATP-triggered release of loads from the microcapsules is of specific interest since ATP is overexpressed in certain cells at different diseases, *e.g.*, cancer. Thus, the targeted release of drugs entrapped in the microcapsules seems feasible. Also, the preparation of the microcapsules by the layer-by-layer deposition process of DNA layers allows the engineering of microcapsules with outer layers that include cell targeting aptamers (*e.g.*, the AS1411 aptamer for targeting cancer cells[65]). The present capsules have a diameter of *ca.* 2.8 $\mu$m. Although these dimensions could hinder the intracellular permeability of the capsules, preliminary studies reveal that the microcapsules bind to breast cancer cells and even permeate into the cells, Figure S7, Supporting Information. Nonetheless, the implementation of smaller cores for the construction of the microcapsules, and eventually, the attachment of targeting aptamer ligand to the outer shell of the microcapsules could further improve the release of payloads in the cells. These issues will be addressed in a follow-up study.

## METHODS

**Reagents and Materials.** Sodium chloride, 4-(2-hydroxyethyl)-piperazine-1-ethanesulfonic acid sodium salt (HEPES base), 4-(2-hydroxyethyl)piperazine-1-ethanesulfonic acid (HEPES acid), magnesium chloride, poly(allylamine hydrochloride) (PAH, 58 kDa MW), ethylenediaminetetraacetic acid disodium salt dihydrate (EDTA), mercaptopropionic acid (MPA), adenosine triphosphate (ATP), guanosine triphosphate (GTP), cytidine triphosphate (CTP), thymidine triphosphate (TTP), hydrogen peroxide ($H_2O_2$) and microperoxidase-11 (MP-11) were purchased from Sigma–Aldrich. Tetramethylrhodamine-dextran (TMR-D, 70 kDa MW) and Amplex UltraRed Reagent were purchased from Life Technologies Corporation. Maple Red-Orange CdSe/ZnS Quantum dots in toluene were purchased from Evident Technologies. All oligonucleotides were synthesized, standard desalting purified, and freeze-dried by Integrated DNA Technologies, Inc. Ultrapure water from a NANOpure Diamond (Barnstead Int., Dubuque, IA) source was used in all experiments.

**Preparation of TMR-D-Loaded $CaCO_3$ Microparticles.** $CaCO_3$ particles were prepared by a precipitation reaction between equal amounts of $CaCl_2$ and $Na_2CO_3$ under magnetic stirring at room temperature, as reported by Volodkin.[66] $CaCO_3$ particles loaded with tetramethylrhodamine-modified dextran, TMR-D, were obtained through coprecipitation by mixing of $CaCl_2$ (300 $\mu$L, 0.33 M) and $Na_2CO_3$ (300 $\mu$L, 0.33 M) solution, in the presence of TMR-D; the ratio of TMR-D and deionized water was adjusted accordingly to obtain a total volume of 1020 $\mu$L and 0.2 $mg \cdot mL^{-1}$ of TMR-D as final concentration. After magnetic stirring for 110 s, the suspension was left for 70 s at room temperature to settle down. The particles were centrifuged at 900 rpm for 20 s, followed by the removal of the supernatant solution, and the subsequent resuspension of the particles in water. This washing procedure was repeated for three times, to remove byproducts resulting from the precipitation reaction. Both CdSe/ZnS QDs-loaded and microperoxidase-11-loaded capsules were prepared by the same method, using coprecipitation procedure. The final concentration of MPA-capped CdSe/ZnS QDs and MP-11 was 0.8 $\mu$M and 2 $mg \cdot mL^{-1}$, respectively.

**Synthesis of Layer-by-Layer (LbL) DNA Assembled Capsules.** $CaCO_3$ microparticles were suspended in 1 $mg \cdot mL^{-1}$ PAH solution (in 10 mM HEPES, pH 7, containing 500 mM NaCl and 50 mM $MgCl_2$) under continuously shaking. After an adsorption time-interval of 20 min, the particles were washed twice with 10 mM HEPES buffer (pH 7, containing 500 mM NaCl) followed by centrifuging at 900 rpm for 20 s. The obtained PAH-modified $CaCO_3$ microparticles were coated by sequential incubation of the particles in DNA hybrid **1**/**2** and **3**/**2** solutions for 30 min [15 $\mu$M in 10 mM HEPES, pH 7, containing 500 mM NaCl and 50 mM $MgCl_2$, the ratio of **1** to **2** and **3** to **2** is 2 to 1]. After each adsorption step, one washing step was performed to remove nonadsorbed nucleic acids. Six layers of nucleic acids were deposited in total. (Only three layers of nucleic acids were deposited in the preparation of the QDs-loaded $CaCO_3$ particles, since six layers of DNA shells were found to be too dense to release QDs.) After the LbL assembly of the DNA shells, the template cores were dissolved by adding 0.5 M EDTA (pH 6) to yield a solution with the final concentration of 0.1 M EDTA for 1 h under gentle rotation. After the suspension became clear, the supernatant EDTA solution was removed through slow centrifugation to avoid aggregation of the DNA capsules. The capsules were washed three times with 10 mM HEPES buffer (pH 7, containing 500 mM NaCl) by centrifuging at 500 rpm for 20 min.

**Characterization of Microparticles.** Confocal fluorescence and bright-field microscopy images of $CaCO_3$ particles and DNA capsules were monitored by using a FV-1000 confocal microscope (Olympus, Japan) equipped with an IX81 inverted microscope. A 60 × /1.3 oil immersion objective was used. SEM images were recorded with a Magellan XHR 400L SEM operated at an acceleration voltage of 3 kV. The formation of capsules was also observed by iCyt Eclipse Analyzer Flow Cytometer

according to the fluorescence intensity changes of the resulting capsules. All the experiments were performed in 10 mM HEPES buffer solution (pH 7) containing 500 mM NaCl.

**ATP-Induced Capsules Unlocking and the Release of the Entrapped Loads.** Experiments were performed using a capsules solution, concentration of 130 capsules/$\mu$L. The capsules solution, 38 $\mu$L, was treated with 2 $\mu$L of ATP (in 10 mM HEPES, pH 7, 500 mM NaCl). After incubation, sample solutions were centrifuged at 500 rpm for 20 min to precipitate the residual capsules, and the fluorescence of the released TMR-D or CdSe/ZnS QDs in the supernatant solution was measured by Cary Eclipse Fluorescence Spectrophotometer (Varian, Inc.). The catalytic activity of the released MP-11 was assayed by incubating 20 $\mu$L of supernatant solution with 100 $\mu$L of HEPES buffer solution, 10 mM, pH 7, containing 500 mM NaCl, in the presence of 100 $\mu$M Amplex UltraRed and 0.1 mM $H_2O_2$.

The contents of the released loads TMR-D, CdSe/ZnS QDs and MP-11 upon the ATP-driven unlocking of the microcapsules were evaluated by deriving appropriate calibration curves, Figure S6, Supporting Information, and evaluating the fluorescence/absorbance features of the released loads on the respective calibration curves.

*Conflict of Interest:* The authors declare no competing financial interest.

*Acknowledgment.* This research was supported by the Minerva Center for Biohybrid Complex Systems (I.W.) and by the German Research Foundation, DFG, Grant PA794/21-1 (W.J.P.). Support from the Council for Higher Education in Israel is acknowledged by W.-C.L.

*Supporting Information Available:* The Supporting Information is available free of charge on the ACS Publications website at DOI: 10.1021/acsnano.5b03223.

SEM image of DNA capsules; control experiment of non-ATP aptamer capsules; optimization of DNA layer number of capsules; confirmation of DNA multilayer assembly and ATP triggered dehybridization by quartz crystal microbalance; determining the concentration of released TMR-D, CdSe/ZnS QDs, and MP-11; imaging the interactions of the CdSe/ZnS QDs-loaded microcapsules with MDA-231 breast cancer cells (PDF)

## REFERENCES AND NOTES

1. Peyratout, C. S.; Dähne, L. Tailor-Made Polyelectrolyte Microcapsules: From Multilayers to Smart Containers. *Angew. Chem., Int. Ed.* **2004**, *43*, 3762–3783.
2. Skirtach, A. G.; Yashchenok, A. M.; Möhwald, H. Encapsulation, Release and Applications of LbL Polyelectrolyte Multilayer Capsules. *Chem. Commun.* **2011**, *47*, 12736–12746.
3. Tong, W.; Song, X.; Gao, C. Layer-by-Layer Assembly of Microcapsules and Their Biomedical Applications. *Chem. Soc. Rev.* **2012**, *41*, 6103–6124.
4. Ochs, M.; Carregal-Romero, S.; Rejman, J.; Braeckmans, K.; De Smedt, S. C.; Parak, W. J. Light-Addressable Capsules as Caged Compound Matrix for Controlled Triggering of Cytosolic Reactions. *Angew. Chem., Int. Ed.* **2013**, *52*, 695–699.
5. Shi, J.; Jiang, Y.; Wang, X.; Wu, H.; Yang, D.; Pan, F.; Su, Y.; Jiang, Z. Design and Synthesis of Organic−Inorganic Hybrid Capsules for Biotechnological Applications. *Chem. Soc. Rev.* **2014**, *43*, 5192–5210.
6. Lvov, Y.; Decher, G.; Moehwald, H. Assembly, Structural Characterization, and Thermal Behavior of Layer-by-Layer Deposited Ultrathin Films of Poly(vinyl sulfate) and Poly(allylamine). *Langmuir* **1993**, *9*, 481–486.
7. Donath, E.; Sukhorukov, G. B.; Caruso, F.; Davis, S. A.; Möhwald, H. Novel Hollow Polymer Shells by Colloid-Templated Assembly of Polyelectrolytes. *Angew. Chem., Int. Ed.* **1998**, *37*, 2201–2205.
8. Caruso, F.; Caruso, R. A.; Möhwald, H. Nanoengineering of Inorganic and Hybrid Hollow Spheres by Colloidal Templating. *Science* **1998**, *282*, 1111–1114.
9. Caruso, F.; Lichtenfeld, H.; Giersig, M.; Möhwald, H. Electrostatic Self-Assembly of Silica Nanoparticle-Polyelectrolyte Multilayers on Polystyrene Latex Particles. *J. Am. Chem. Soc.* **1998**, *120*, 8523–8524.
10. Antipov, A. A.; Sukhorukov, G. B.; Leporatti, S.; Radtchenko, I. L.; Donath, E.; Möhwald, H. Polyelectrolyte Multilayer Capsule Permeability Control. *Colloids Surf., A* **2002**, *198*, 535–541.
11. Zhu, Y.; Tong, W.; Gao, C. Molecular-Engineered Polymeric Microcapsules Assembled from Concanavalin A and Glycogen with Specific Responses to Carbohydrates. *Soft Matter* **2011**, *7*, 5805–5815.
12. Connal, L. A.; Kinnane, C. R.; Zelikin, A. N.; Caruso, F. Stabilization and Functionalization of Polymer Multilayers and Capsules *via* Thiol-Ene Click Chemistry. *Chem. Mater.* **2009**, *21*, 576–578.
13. Ochs, C. J.; Such, G. K.; Yan, Y.; van Koeverden, M. P.; Caruso, F. Biodegradable Click Capsules with Engineered Drug-Loaded Multilayers. *ACS Nano* **2010**, *4*, 1653–1663.
14. Becker, A. L.; Zelikin, A. N.; Johnston, A. P.; Caruso, F. Tuning the Formation and Degradation of Layer-by-Layer Assembled Polymer Hydrogel Microcapsules. *Langmuir* **2009**, *25*, 14079–14085.
15. Radt, B.; Smith, T. A.; Caruso, F. Optically Addressable Nanostructured Capsules. *Adv. Mater.* **2004**, *16*, 2184–2189.
16. Angelatos, A. S.; Radt, B.; Caruso, F. Light-Responsive Polyelectrolyte/Gold Nanoparticle Microcapsules. *J. Phys. Chem. B* **2005**, *109*, 3071–3076.
17. Skirtach, A. G.; Dejugnat, C.; Braun, D.; Susha, A. S.; Rogach, A. L.; Parak, W. J.; Möhwald, H.; Sukhorukov, G. B. The Role of Metal Nanoparticles in Remote Release of Encapsulated Materials. *Nano Lett.* **2005**, *5*, 1371–1377.
18. Skirtach, A. G.; Muñoz Javier, A.; Kreft, O.; Köhler, K.; Piera Alberola, A.; Möhwald, H.; Parak, W. J.; Sukhorukov, G. B. Laser-Induced Release of Encapsulated Materials inside Living Cells. *Angew. Chem., Int. Ed.* **2006**, *45*, 4612–4617.
19. Barman, A. K.; Verma, S. Sunlight Mediated Disruption of Peptide-Based Soft Structures Decorated with Gold Nanoparticles. *Chem. Commun.* **2010**, *46*, 6992–6994.
20. Carregal-Romero, S.; Guardia, P.; Yu, X.; Hartmann, R.; Pellegrino, T.; Parak, W. J. Magnetically Triggered Release of Molecular Cargo from Iron Oxide Nanoparticle Loaded Microcapsules. *Nanoscale* **2015**, *7*, 570–576.
21. De Geest, B. G.; Skirtach, A. G.; Mamedov, A. A.; Antipov, A. A.; Kotov, N. A.; De Smedt, S. C.; Sukhorukov, G. B. Ultrasound-Triggered Release from Multilayered Capsules. *Small* **2007**, *3*, 804–808.
22. Kolesnikova, T. A.; Gorin, D. A.; Fernandes, P.; Kessel, S.; Khomutov, G. B.; Fery, A.; Shchukin, D. G.; Möhwald, H. Nanocomposite Microcontainers with High Ultrasound Sensitivity. *Adv. Funct. Mater.* **2010**, *20*, 1189–1195.
23. Pavlov, A. M.; Saez, V.; Cobley, A.; Graves, J.; Sukhorukov, G. B.; Mason, T. J. Controlled Protein Release from Microcapsules with Composite Shells Using High Frequency Ultrasound-Potential for *in Vivo* Medical Use. *Soft Matter* **2011**, *7*, 4341–4347.
24. del Mercato, L. L.; Gonzalez, E.; Abbasi, A. Z.; Parak, W. J.; Puntes, V. Synthesis and Evaluation of Gold Nanoparticle-Modified Polyelectrolyte Capsules under Microwave Irradiation for Remotely Controlled Release for Cargo. *J. Mater. Chem.* **2011**, *21*, 11468–11471.
25. Lu, Z.; Prouty, M. D.; Guo, Z.; Golub, V. O.; Kumar, C. S.; Lvov, Y. M. Magnetic Switch of Permeability for Polyelectrolyte Microcapsules Embedded with Co@Au Nanoparticles. *Langmuir* **2005**, *21*, 2042–2050.
26. Shiratori, S. S.; Rubner, M. F. pH-Dependent Thickness Behavior of Sequentially Adsorbed Layers of Weak Polyelectrolytes. *Macromolecules* **2000**, *33*, 4213–4219.
27. Lutkenhaus, J. L.; McEnnis, K.; Hammond, P. T. Tuning the Glass Transition of and Ion Transport within Hydrogen-Bonded Layer-by-Layer Assemblies. *Macromolecules* **2007**, *40*, 8367–8373.
28. Hartmann, L.; Bedard, M.; Börner, H. G.; Möhwald, H.; Sukhorukov, G. B.; Antonietti, M. $CO_2$-Switchable Oligoamine Patches Based on Amino Acids and Their Use to Build

Polyelectrolyte Containers with Intelligent Gating. *Soft Matter* **2008**, *4*, 534–539.
29. Levy, T.; Dejugnat, C.; Sukhorukov, G. B. Polymer Microcapsules with Carbohydrate-Sensitive Properties. *Adv. Funct. Mater.* **2008**, *18*, 1586–1594.
30. Zelikin, A. N.; Li, Q.; Caruso, F. Degradable Polyelectrolyte Capsules Filled with Oligonucleotide Sequences. *Angew. Chem., Int. Ed.* **2006**, *45*, 7743–7745.
31. De Geest, B. G.; Vandenbroucke, R. E.; Guenther, A. M.; Sukhorukov, G. B.; Hennink, W. E.; Sanders, N. N.; Demeester, J.; De Smedt, S. C. Intracellularly Degradable Polyelectrolyte Microcapsules. *Adv. Mater.* **2006**, *18*, 1005–1009.
32. Rivera-Gil, P.; De Koker, S.; De Geest, B. G.; Parak, W. J. Intracellular Processing of Proteins Mediated by Biodegradable Polyelectrolyte Capsules. *Nano Lett.* **2009**, *9*, 4398–4402.
33. Ochs, C. J.; Such, G. K.; Caruso, F. Modular Assembly of Layer-by-Layer Capsules with Tailored Degradation Profiles. *Langmuir* **2011**, *27*, 1275–1280.
34. Reibetanz, U.; Chen, M. H. A.; Mutukumaraswamy, S.; Liaw, Z. Y.; Oh, B. H. L.; Donath, E.; Neu, B. Functionalization of Calcium Carbonate Microparticles as a Combined Sensor and Transport System for Active Agents in Cells. *J. Biomater. Sci., Polym. Ed.* **2011**, *22*, 1845–1859.
35. del Mercato, L. L.; Abbasi, A. Z.; Ochs, M.; Parak, W. J. Multiplexed Sensing of Ions with Barcoded Polyelectrolyte Capsules. *ACS Nano* **2011**, *5*, 9668–9674.
36. Balabushevich, N. G.; Sukhorukov, G. B.; Larionova, N. I. Polyelectrolyte Multilayer Microspheres as Carriers for Bienzyme System: Preparation and Characterization. *Macromol. Rapid Commun.* **2005**, *26*, 1168–1172.
37. Stein, E. W.; Volodkin, D. V.; McShane, M. J.; Sukhorukov, G. B. Real-Time Assessment of Spatial and Temporal Coupled Catalysis within Polyelectrolyte Microcapsules Containing Coimmobilized Glucose Oxidase and Peroxidase. *Biomacromolecules* **2006**, *7*, 710–719.
38. Skirtach, A. G.; De Geest, B. G.; Mamedov, A.; Antipov, A. A.; Kotov, N. A.; Sukhorukov, G. B. Ultrasound Stimulated Release and Catalysis Using Polyelectrolyte Multilayer Capsules. *J. Mater. Chem.* **2007**, *17*, 1050–1054.
39. de Villiers, M. M.; Lvov, Y. M. Layer-by-Layer Self-Assembled Nanoshells for Drug Delivery. *Adv. Drug Delivery Rev.* **2011**, *63*, 699–700.
40. Shchukina, E. M.; Shchukin, D. G. LbL Coated Microcapsules for Delivering Lipid-Based Drugs. *Adv. Drug Delivery Rev.* **2011**, *63*, 837–846.
41. Becker, A. L.; Orlotti, N. I.; Folini, M.; Cavalieri, F.; Zelikin, A. N.; Johnston, A. P.; Zaffaroni, N.; Caruso, F. Redox-Active Polymer Microcapsules for the Delivery of a Survivin-Specific siRNA in Prostate Cancer Cells. *ACS Nano* **2011**, *5*, 1335–1344.
42. Ai, H. Layer-by-Layer Capsules for Magnetic Resonance Imaging and Drug Delivery. *Adv. Drug Delivery Rev.* **2011**, *63*, 772–788.
43. Johnston, A. P.; Read, E. S.; Caruso, F. DNA Multilayer Films on Planar and Colloidal Supports: Sequential Assembly of Like-Charged Polyelectrolytes. *Nano Lett.* **2005**, *5*, 953–956.
44. Johnston, A. P.; Mitomo, H.; Read, E. S.; Caruso, F. Compositional and Structural Engineering of DNA Multilayer Films. *Langmuir* **2006**, *22*, 3251–3258.
45. Lee, L.; Johnston, A. P.; Caruso, F. Manipulating the Salt and Thermal Stability of DNA Multilayer Films *via* Oligonucleotide Length. *Biomacromolecules* **2008**, *9*, 3070–3078.
46. Fujii, A.; Maruyama, T.; Ohmukai, Y.; Kamio, E.; Sotani, T.; Matsuyama, H. Cross-Linked DNA Capsules Templated on Porous Calcium Carbonate Microparticles. *Colloids Surf., A* **2010**, *356*, 126–133.
47. Wang, F.; Liu, X.; Willner, I. DNA Switches: From Principles to Applications. *Angew. Chem., Int. Ed.* **2015**, *54*, 1098–1129.
48. Johnston, A. P.; Lee, L.; Wang, Y.; Caruso, F. Controlled Degradation of DNA Capsules with Engineered Restriction-Enzyme Cut Sites. *Small* **2009**, *5*, 1418–1421.
49. Tombelli, S.; Minunni, M.; Mascini, M. Analytical Applications of Aptamers. *Biosens. Bioelectron.* **2005**, *20*, 2424–2434.
50. Willner, I.; Zayats, M. Electronic Aptamer-Based Sensors. *Angew. Chem., Int. Ed.* **2007**, *46*, 6408–6418.
51. Mairal, T.; Özalp, V. C.; Sánchez, P. L.; Mir, M.; Katakis, I.; O'Sullivan, C. K. Aptamers: Molecular Tools for Analytical Applications. *Anal. Bioanal. Chem.* **2008**, *390*, 989–1007.
52. Liu, J.; Cao, Z.; Lu, Y. Functional Nucleic Acid Sensors. *Chem. Rev.* **2009**, *109*, 1948–1998.
53. Teller, C.; Shimron, S.; Willner, I. Aptamer-DNAzyme Hairpins for Amplified Biosensing. *Anal. Chem.* **2009**, *81*, 9114–9119.
54. Zhang, M.; Huang, J.; Deng, M.; Weng, X.; Ma, H.; Zhou, X. Sensitive and Visual Detection of Adenosine by a Rationally Designed FokI-Based Biosensing Strategy. *Chem. - Asian J.* **2009**, *4*, 1420–1423.
55. Zhu, Z.; Wu, C.; Liu, H.; Zou, Y.; Zhang, X.; Kang, H.; Yang, C. J.; Tan, W. An Aptamer Cross-Linked Hydrogel as a Colorimetric Platform for Visual Detection. *Angew. Chem.* **2010**, *122*, 1070–1074.
56. Zhang, Z.; Balogh, D.; Wang, F.; Willner, I. Smart Mesoporous $SiO_2$ Nanoparticles for the DNAzyme-Induced Multiplexed Release of Substrates. *J. Am. Chem. Soc.* **2013**, *135*, 1934–1940.
57. Zhang, Z.; Balogh, D.; Wang, F.; Sung, S. Y.; Nechushtai, R.; Willner, I. Biocatalytic Release of an Anticancer Drug from Nucleic-Acids-Capped Mesoporous $SiO_2$ Using DNA or Molecular Biomarkers as Triggering Stimuli. *ACS Nano* **2013**, *7*, 8455–8468.
58. Sultan, Y.; DeRosa, M. C. Target Binding Influences Permeability in Aptamer-Polyelectrolyte Microcapsules. *Small* **2011**, *7*, 1219–1226.
59. Zhang, X.; Chabot, D.; Sultan, Y.; Monreal, C.; DeRosa, M. C. Target-Molecule-Triggered Rupture of Aptamer-Encapsulated Polyelectrolyte Microcapsules. *ACS Appl. Mater. Interfaces* **2013**, *5*, 5500–5507.
60. Malile, B.; Chen, J. I. Morphology-Based Plasmonic Nanoparticle Sensors: Controlling Etching Kinetics with Target-Responsive Permeability Gate. *J. Am. Chem. Soc.* **2013**, *135*, 16042–16045.
61. Cole, S.; Bhardwaj, G.; Gerlach, J.; Mackie, J.; Grant, C.; Almquist, K.; Stewart, A.; Kurz, E.; Duncan, A.; Deeley, R. Overexpression of a Transporter Gene in a Multidrug-Resistant Human Lung Cancer Cell Line. *Science* **1992**, *258*, 1650–1654.
62. Devenish, R. J.; Prescott, M.; Boyle, G. M.; Nagley, P. The Oligomycin Axis of Mitochondrial ATP Synthase: OSCP and the Proton Channel. *J. Bioenerg. Biomembr.* **2000**, *32*, 507–515.
63. del Mercato, L. L.; Abbasi, A. Z.; Parak, W. J. Synthesis and Characterization of Ratiometric Ion-Sensitive Polyelectrolyte Capsules. *Small* **2011**, *7*, 351–363.
64. Kagan, V. E.; et al. Cytochrome c Acts as a Cardiolipin Oxygenase Required for Release of Proapoptotic Factors. *Nat. Chem. Biol.* **2005**, *1*, 223–232.
65. Bates, P. J.; Kahlon, J. B.; Thomas, S. D.; Trent, J. O.; Miller, D. M. Antiproliferative Activity of G-rich Oligonucleotides Correlates with Protein Binding. *J. Biol. Chem.* **1999**, *274*, 26369–26377.
66. Volodkin, D. V.; Petrov, A. I.; Prevot, M.; Sukhorukov, G. B. Matrix Polyelectrolyte Microcapsules: New System for Macromolecule Encapsulation. *Langmuir* **2004**, *20*, 3398–3406.